



Letter

Hydrogen effects on stainless steel passive film fracture studied by nanoindentation

Y. Yao^{a,b}, L.J. Qiao^{a,*}, Alex A. Volinsky^{a,c,1}^a Corrosion and Protection Center, Key Laboratory for Environmental Fracture (MOE), University of Science and Technology Beijing, Beijing 100083, People's Republic of China^b Department of Materials Science and Engineering, Hainan University, Hainan Province 570228, People's Republic of China^c Department of Mechanical Engineering, University of South Florida, 4202 E. Fowler Ave., ENB118, Tampa, FL 33620, USA

ARTICLE INFO

Article history:

Received 12 April 2011

Accepted 7 May 2011

Available online 12 May 2011

Keywords:

A. Stainless steel

B. AFM

C. Passive films

C. Hydrogen absorption

ABSTRACT

Hydrogen effects on the fracture stress of passive film formed on 316L stainless steel were studied by nanoindentation. Hydrogen accumulated primarily on the sample surface and in the passive film. Displacement excursion related to film fracture appeared in load-controlled load–displacement curves when electrochemically polished and anodically passivated samples were indented. The excursion disappeared after the passivation film was removed electrochemically or by nanowear. The critical load, excursion depth and length decreased with higher hydrogen concentration, along with Young's modulus and fracture stress of the passive film.

© 2011 Elsevier Ltd. All rights reserved.

1. Introduction

Many commonly used metals and alloys, such as stainless steel (SS), corrode with passive film forming due to aqueous solution exposure. Reduction of hydrogen ions is the most common reaction that accompanies aqueous corrosion of metals. During corrosion processes part of the reduced hydrogen can absorb on the metal surface and diffuse into corroding material [1–4], while the rest of hydrogen forms gas molecules and escapes. Hydrogen dissolved in metals significantly affects their mechanical properties, composition and structure of passive films. For instance, hydrogen can cause low yield and fracture stresses in steels [5–7]. Studies showed that hydrogen affects steel corrosion rates [1,8–10], stress corrosion cracking (SCC) [11–13] and pitting [14–16]. For 310 SS, no pitting corrosion occurred in 6% FeCl₃ solution for more than 150 h. However, pitting occurred within 80 min when 310 SS was pre-charged with hydrogen at very low 1 A/m² current density [15]. Susceptibility to SCC and pitting of SS are closely related to mechanical properties of the passive film, therefore, it is important to study hydrogen effects on the passive film mechanical properties and fracture.

Nanoindentation has been extensively used to study mechanical properties of thin and passive films on metal and alloy surfaces [17,18]. A displacement discontinuity (excursion) was observed in load–displacement curves during load-controlled nanoindentation of electropolished tungsten [19], Fe–3% Si [20], single crystal stainless steel [21], nickel [22], and austenitic stainless steel [23]. Prior

to this excursion indentation was elastic, fully recoverable, with almost no difference between the loading and the unloading portions of the load–displacement curve. After this excursion, material exhibited plastic deformation [19,24,25], therefore, displacement excursions were ascribed to the onset of plasticity in the oxide film on tungsten and Fe–3% Si surfaces [19,20]. On the other hand, indentation displacement excursions at low loads have also been observed in electropolished nickel [17], sputtered aluminum films [26], anodic passive film on titanium [27] and air-formed film on Fe–3% Si [29]. These excursions were ascribed to film fracture as the sample permanently deformed prior to the displacement excursion. When the oxide film on electropolished surfaces was removed by immersion in 5% HCl [20], or indentation was carried out in 1 M H₂SO₄ solution [28], no excursions happened.

The excursion load, P_0 , excursion depth, δ_0 , and excursion length, δ_{ex} , are the major parameters of the load-controlled nanoindentation excursion event. If the excursion is ascribed to the onset of plasticity, the yield stress of the oxide film can be calculated based on the excursion load, P_0 . Calculated yield stress was between 1 and 4 GPa [18,28]. The number of dislocations generated underneath an indenter tip is related to the excursion length, δ_{ex} [18]. If the excursion is ascribed to film fracture, the fracture stress of the oxide or passive film can be calculated based on the excursion critical load, P_0 [27].

Hydrogen affects metal mechanical properties, including Young's modulus, yield and fracture stresses [30–33]. Hydrogen can also influence passive film mechanical properties. However, there are few reports considering hydrogen effects on the passive film mechanical properties. The research objective of this paper is to investigate the effect of hydrogen on Young's modulus and fracture stress of the passive film.

* Corresponding author. Tel.: +86 10 6233 4499; fax: +86 10 6233 2345.

E-mail addresses: lqiao@ustb.edu.cn (L.J. Qiao), volinsky@eng.usf.edu (A.A. Volinsky).¹ Tel.: +1 813 974 5658; fax: +1 813 974 3539.

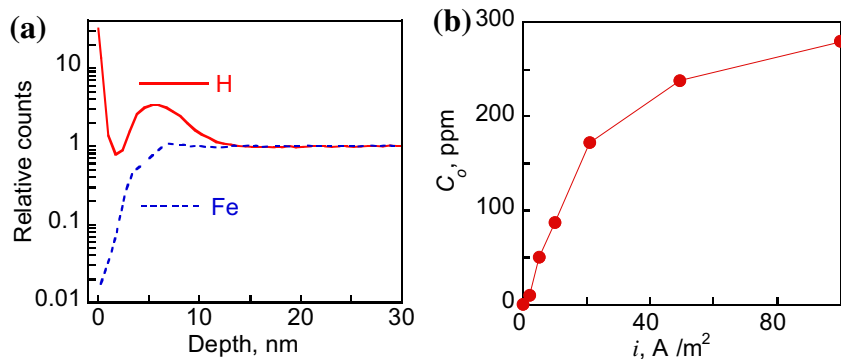


Fig. 1. (a) TOF-SIMS hydrogen and iron depth profiles of the sample charged at 20 A/m² current density. (b) Hydrogen concentration, C_0 , vs. charging current density, i .

2. Experimental procedure

Type 316 austenitic stainless steel used in this study had the following composition in weight percent: 17.05% Cr, 11.15% Ni, 2.17% Mo, 1.43% Mn, 0.53% Si, 0.13% S, 0.025% P, 0.022% C, and Fe balanced. Disk specimens with 16 mm diameter, 2 mm thick were heat treated at 1050 °C for 1 h followed by water quenching to obtain austenite structure and dissolve inclusions, primarily carbides. All specimens were wet ground to a 1000-grit, and then electropolished in a mixture of 56% H₃PO₄ + 40% H₂SO₄ + 2% CrO₃ + 2% H₂O at 25 V with a platinum cathode.

Specimens were charged with hydrogen for 10 h at room temperature in 0.5 mol/L H₂SO₄ + 0.25 g/L As₂O₃ solution with 20, 50, 100, 200 and 500 A/m² current densities, respectively. Hydrogen concentration was calculated based on the gas volume escaped from the sample measured in a collection glass tube filled with silicone oil. The amount of hydrogen in moles evolved from the sample can be determined from the ideal gas law. Since one mole of H₂ weighs 2.016 g, hydrogen concentration in steel specimens, C_0 , in parts per million by weight (ppm), can be calculated based on the measured hydrogen volume, V (m³), evolved at room temperature, T (293.16 K) and atmospheric pressure, P (101,325 Pa):

$$C_0 = \frac{10^6 PV}{m RT} = 2.45682 \times 10^7 \frac{V}{mT} \quad (1)$$

Here, R is the gas constant (8.314472 J mol⁻¹ K⁻¹), and m is the steel specimen weight in kg. The sample was kept in the collection glass tube filled with silicone oil until hydrogen stopped escaping from the sample. Although not performed in this paper, hydrogen evolution rate can be increased by raising the sample temperature to 100–150 °C, since diffusion rate has exponential temperature dependence.

To remove surface oxide film before passivation, specimens' potential was swept dynamically in a borate buffer solution (0.02 M H₃BO₃ + 0.005 M Na₂B₄O₇·10H₂O) from -1200 to 400 mV_{SCE} at 0.5 mV/s rate. Samples with different amounts of hydrogen were then held at 400 mV_{SCE} potential for 6 h to form passive film. There is more hydrogen on the sample surface and in the passive film, based on the depth profile obtained from the time of flight secondary ion mass spectrometry (TOF-SIMS) results shown in Fig. 1a for the sample charged at 20 A/m² current density. The sample was analyzed 3 h after hydrogen charging. The data was normalized by the bulk values to illustrate that there is more hydrogen on the sample surface and in the film. Surface adsorption is responsible for the highest detected hydrogen concentration at the sample surface. In the film the maximum relative hydrogen concentration is at 5 nm depth, and decays at 10 nm, suggesting that the passive film is less than 10 nm thick. Hydrogen concentration in the charged samples as a function of the current density is shown in Fig. 1b.

Nanoindentation tests were performed immediately after passivation with the Hysitron Triboscope nanoindenter mounted onto DI3100 atomic force microscope. Berkovich indenter with 150 nm tip radius was used with loading rates between 50 and 500 μN/s.

3. Results and discussion

3.1. Yield and fracture phenomena during indentation

A typical load–depth curve for the electropolished specimens is shown as curve A in Fig. 2a. The loading–unloading portions of the load–depth curves overlay for the indents with a maximum load less than P_0 in Fig. 2a, curve A, meaning that no permanent deformation occurred. At the same time, topography image of the corresponding indented region with load less than P_0 shows no residual

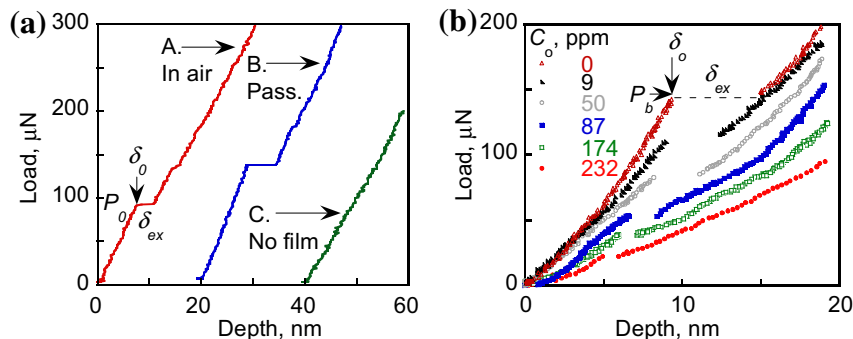


Fig. 2. (a) Load–displacement curves during nanoindentation of electropolished 316L stainless steel with the oxide film formed: (A) in air, (B) passivated, and (C) film removed. Curves are offset horizontally for clarity; (b) load–depth curves corresponding to varying hydrogen concentration, C_0 .

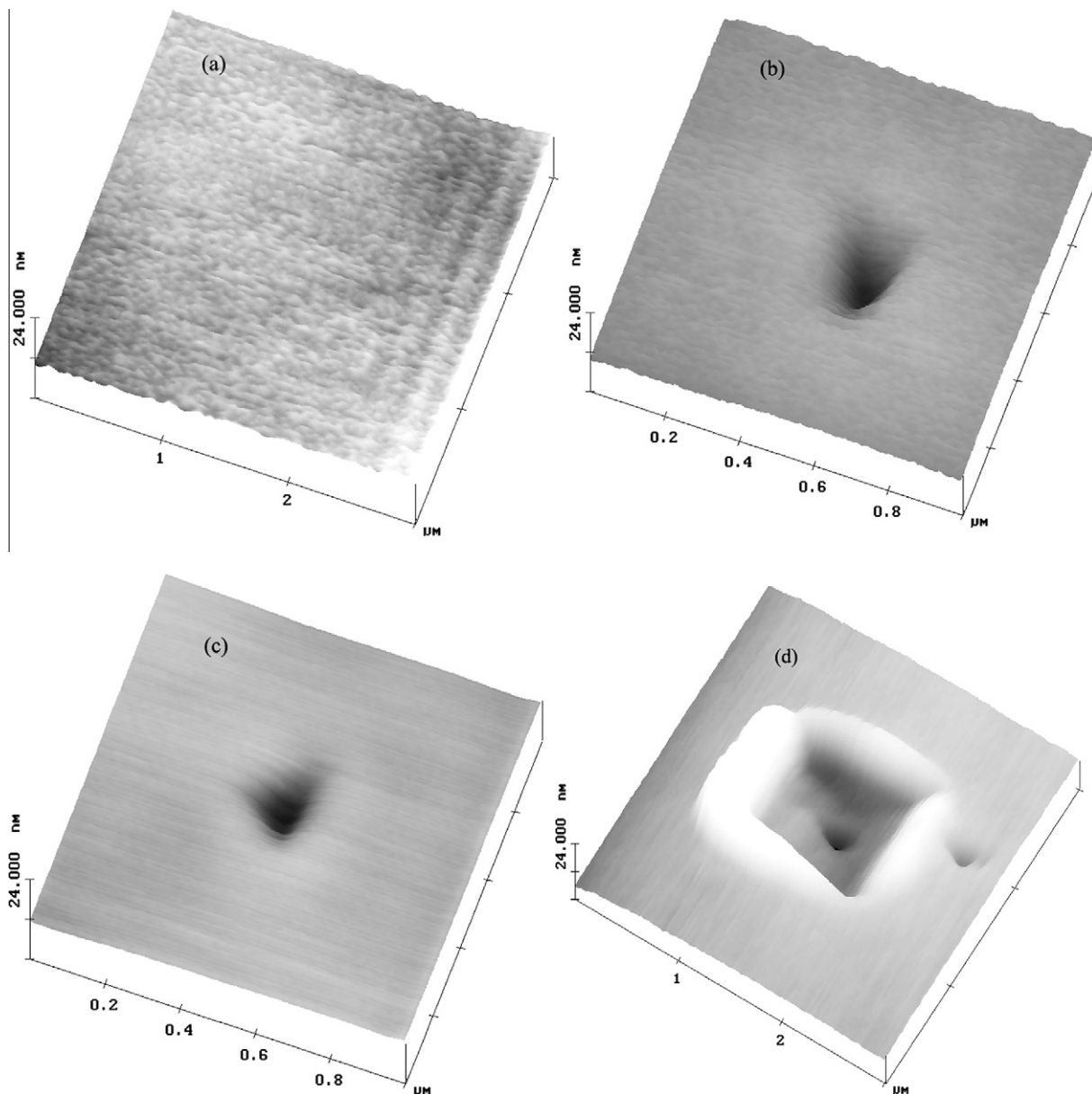


Fig. 3. Topography images of residual indentation marks: (a) below P_{cr} in Fig. 1a; (b) passivation film; (c) no film, corresponding to B and C load–depth curves in Fig. 1a, and (d) topography image of the nanowear indented region.

deformation mark in Fig. 3a. However, the load–displacement curve revealed permanent deformation for the indent with a maximum load larger than P_0 in the curve B of Fig. 2a. In this case, topography image of the corresponding indent reveals residual impression, seen in Fig. 3b. Indentations of electropolished specimens exhibited displacement excursions, since all electropolished specimens have surface film. After the surface film was worn off using nanowear function of the Hysitron Triboscope (350 wear cycles at 50 μN normal load), indentation of the worn region did not reveal the displacement excursion in Fig. 2a, curve C. When the surface film was removed by potential dynamic sweeping from -1200 to 400 mV_{SCE} in the borate buffer solution and immediately indented, no displacement excursion was observed as well.

Typical load–displacement curve of the specimen with anodic passivation film formed at 400 mV_{SCE} anodic potential held for 6 h is shown as curve B in Fig. 2a. Comparing curves A and B in Fig. 2a, the excursion load for the specimens with the anodic passive film is higher than that for the electropolished specimen. Anodic passive film (curve B in Fig. 2a) exhibits permanent

Table 1

Average values of six measurements of the passive film breaking load, P_b , excursion depth, δ_0 , excursion length, δ_{ex} , Young's modulus, E_s , and breaking stress, σ_b , with the corresponding varied hydrogen concentration, C_0 .

i	A/m ²	0	20	50	100	200	500
C_0	ppm by wt	0	9.68	50.37	87.18	174.36	232.48
P_b	μN	143	117	85	58	41	24
δ_0	nm	8.3	7.9	7.1	6.4	5.7	5.2
δ_{ex}	nm	5.5	4.5	3.45	1.5	0.8	0.5
E_s	GPa	248	224	201	169	150	106
σ_b	GPa	4.7	4.05	3.24	2.67	2.24	1.74

deformation with corresponding topography image in Fig. 3b revealing residual indentation mark. Therefore, displacement excursion during indentation was caused by the film breaking and the critical load of the excursion, P_0 , is the fracture load of the passive film, P_b . The breaking load, P_b , excursion depth, δ_0 , and length, δ_{ex} , of the passive film are listed in Table 1 (average values of six measurements). The load–depth curves of the worn region where the anodic passivation film has been removed do not

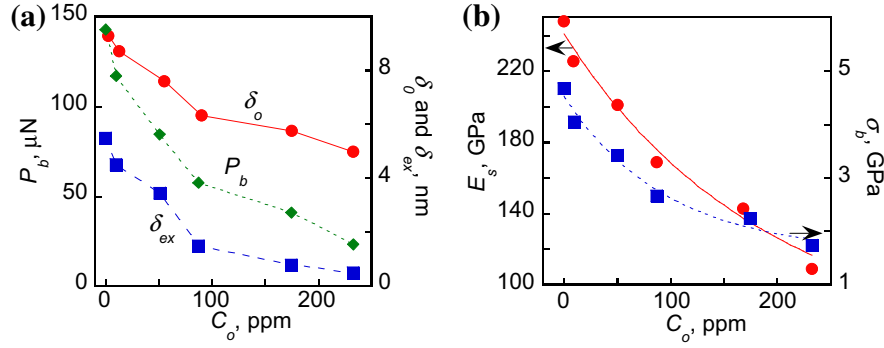


Fig. 4. (a) Hydrogen concentration effect on the excursion depth, δ_o , length, δ_{ex} , the critical load, P_b ; (b) hydrogen concentration effects on the fracture stress, σ_b , and reduced elastic modulus, E_s , of the passive film. Data are fitted with corresponding Eqs. (5) and (6).

exhibit the excursion, as seen in curve C of Fig. 2a. Topography image of the worn region with indents is shown in Fig. 3d. No excursions occurred during nanoindentation of 316 stainless steel with the surface film removed. Displacement excursions in 316 stainless steel are ascribed to film fracture formed during electropolishing in air, or electrochemically at passivation potential.

3.2. Hydrogen effect on the passive film fracture

Concentration of hydrogen, C_o , evolved at room temperature under various current densities, i , is shown in Fig. 1b and listed in Table 1. Typical load–depth curves during indentation into anodic passivated specimens with varying hydrogen concentration are shown in Fig. 2b. The breaking load P_b , excursion depth, δ_o , and excursion length, δ_{ex} , of the anodic passivation film with various hydrogen concentrations are also listed in Table 1. Table 1 indicates that the breaking load, P_b , the excursion depth, δ_o , and the excursion length, δ_{ex} , decrease with hydrogen concentration, C_o , as seen in Fig. 2b.

With less than 10 nm excursion depth, δ_o , indentation with the 150 nm tip radius Berkovich indenter is within the spherical contact region. According to Hertzian contact mechanics, the maximum radial tensile stress in the film at the very edge of the spherical contact surface, responsible for the film fracture, is [27,28]:

$$\sigma = \frac{(1 - 2\nu_s)}{3} \left(\frac{6E_r^2 P}{\pi^3 r^2} \right)^{1/3} \quad (2)$$

where ν_s is the Poisson's ratio of the specimen, P is the applied load, r is the radius of the indenter tip, and E_r is the effective Young's modulus of the sample and the tip, defined as [25]:

$$\frac{1}{E_r} = \frac{(1 - \nu_s^2)}{E_s} + \frac{(1 - \nu_i^2)}{E_i} \quad (3)$$

where E_s and E_i , ν_s and ν_i are the Young's modulus and Poisson's ratios of the specimen and the indenter tip, respectively. For the diamond tip, $E_i = 1140$ GPa and $\nu_i = 0.07$, therefore the effective Young's modulus is approximately equal to that of the stainless steel specimen. Based on the load (P)–depth (δ) curve, E_s is [20]:

$$E_s = \frac{P}{8.3\delta^2} \quad (\text{Hertzian}) \quad (4)$$

$$E_s = \frac{P}{11.12\delta^2} \quad (\text{Love}) \quad (5)$$

For the hydrogen-free sample, substituting the excursion load, P_b , and depth, δ_o , corresponding to the beginning of the excursion into Eqs. (4) and (5), respectively, yields $E_s = 248$ and 187 GPa. For 316 stainless steel used in the study, the Young's modulus is

195 GPa. The modulus of the passive film is greater than that of the SS substrate, thus Eq. (4) was used to illustrate the effect of hydrogen on the Young's modulus. Fig. 4a shows that P_b , δ_{ex} and δ_o all decrease with hydrogen concentration. Based on Eq. (4) or (5), this means that the Young's modulus, E_s , decreases with hydrogen concentration. The depth δ_o , corresponding to the onset of the excursion from Fig. 2b is presented in Fig. 4a and Table 1. By substituting P_b and δ_o values from Table 1 into Eq. (4), E_s was calculated for various hydrogen concentrations, also listed in Table 1.

The breaking stress, σ_b , of the anodic passive film was calculated using Eq. (2) based on P_b and E_r data listed in Table 1 for various hydrogen concentrations. Variations of σ_b and E_s with hydrogen concentration are shown in Fig. 4b. Both E_s and σ_b decrease with hydrogen concentration, i.e.:

$$E = 100 + 140e^{-8 \times 10^{-3} C_o} \quad (6)$$

$$\sigma_0 = 1.5 + 3e^{-9.6 \times 10^{-3} C_o} \quad (7)$$

where, E and σ_0 are in GPa.

Hydrogen in stainless steel could change the composition and/or thickness of the passive film. The critical load of the excursion increased with the film thickness [26,27]. It is challenging to directly measure the passive film thickness, which is on the order of several to tens of nanometers. For the 20 A/m² charged sample the passive film is less than 10 nm thick according to the TOF-SIMS hydrogen and iron profiles shown in Fig. 1a. Young's modulus, E_s , is independent of the film thickness. Fig. 4b shows that E_s evidently decreases with hydrogen concentration, along with the passive film breaking stress, σ_b . Young's modulus is related to the cohesive strength [31]. Therefore, hydrogen reduces E_s and cohesive strength between the SS matrix and the passive film. Stainless steel susceptibility to SCC in several solutions is related to passive film properties [31–34], such as strength and adhesion. If the passive film can be easily broken, the susceptibility to SCC will be higher. Results presented in this paper show that the passive film fracture stress decreases with hydrogen concentration. This is consistent with the effect of hydrogen on stainless steel SCC susceptibility in hot MgCl₂ solution [11]. Hydrogen effect on the passive film fracture is one of the reasons hydrogen facilitates SCC of stainless steels [31].

4. Conclusions

- (1) Hydrogen primarily accumulated on the sample surface and in the passive film.
- (2) The displacement excursion in the load-controlled load–depth nanoindentation curve is caused by the passive film fracture rather than dislocations emission in 316 stainless steel.

- (3) Hydrogen decreased passive film breaking load, excursion depth and length.
- (4) Hydrogen decreased the Young's modulus and the fracture stress of the passive film.

Acknowledgments

Authors thank Ziqiang Qin for the TOF-SIMS data. This work was supported by the National Natural Science Foundation of China (Grant Nos.: 50731003 and 10776001) and Beijing Municipal Science & Technology Commission (Grant No.: D09030303790901). Alex Volinsky acknowledges support from the National Science Foundation under 1000138 and 0966248 grants.

References

- [1] H. Gray, Ion and laser microprobes applied to measurement of corrosion produced hydrogen on a microscopic scale, *Corrosion* 18 (1972) 47.
- [2] L.J. Qiao, W.Y. Chu, C.M. Hsiao, The concentration of hydrogen at crack tip of austenitic stainless steel after stress corrosion and polarization, *Scr. Metall.* 22 (1988) 627–630.
- [3] L.J. Qiao, J.L. Luo, X. Mao, Hydrogen evolution and enrichment around stress corrosion crack tips of pipeline steels in dilute bicarbonate solution, *Corrosion* 54 (1998) 115–121.
- [4] Y.P. Kim, M. Fregonese, H. Mazille, D. Feron, G. Santarini, Study of oxygen reduction on stainless steel surfaces and its contribution to acoustic emission recorded during corrosion processes, *Corros. Sci.* 48 (2006) 3945–3959.
- [5] P.G. Marsh, W.W. Gerberich, in: R.H. Jones (Ed.), *Stress Corrosion Cracking*, ASM International, Ohio, 1992, p. 63.
- [6] G.E. Kerns, M.T. Wang, R.W. Staehle, in: R.W. Staehle (Ed.), *Stress Corrosion Cracking and Hydrogen Embrittlement of Iron Alloys*, NACE, Houston, TX, 1977, p. 700.
- [7] Y. Mine, K. Hirashita, M. Matsuda, M. Otsu, K. Takashima, Effect of hydrogen on tensile behaviour of micrometre-sized specimen fabricated from a metastable austenitic stainless steel, *Corros. Sci.* 53 (2011) 529–533.
- [8] L.J. Qiao, J.L. Luo, Hydrogen-facilitated anodic dissolution of austenitic stainless steels, *Corrosion* 54 (1998) 281–289.
- [9] M. Hasegawa, M. Osawa, Anomalous corrosion of hydrogen-containing ferritic steels in aqueous acid-solution, *Corrosion* 39 (1983) 115–120.
- [10] O.M. Alyousif, R. Nishimura, Stress corrosion cracking and hydrogen embrittlement of sensitized austenitic stainless steels in boiling saturated magnesium chloride solutions, *Corros. Sci.* 50 (2008) 2353–2359.
- [11] L.J. Qiao, W. Chu, H. Miao, J.M. Xiao, P. Guo, Hydrogen-facilitated corrosion and stress corrosion cracking of austenitic stainless steel of type 310, *Metall. Trans. A* 24 (1993) 959–962.
- [12] H.P. Kim, R.H. Song, S.I. Pyun, Effects of hydrogen recombination poisons on stress corrosion crack initiation and propagation in Al–Zn–Mg alloys, *Br. Corros. J.* 23 (1998) 254–258.
- [13] O.M. Alyousif, R. Nishimura, On the stress corrosion cracking and hydrogen embrittlement of sensitized austenitic stainless steels in boiling saturated magnesium chloride solutions: effect of applied stress, *Corros. Sci.* 50 (2008) 2919–2926.
- [14] M.E. Armacanqui, R.A. Oriani, Effect of hydrogen on the pitting resistance of passivating film on nickel in chloride-containing solution, *Corrosion* 44 (1998) 696–698.
- [15] Q. Yang, L.J. Qiao, S. Chiovelli, J.L. Luo, Effects of hydrogen on pitting susceptibility of type 310 stainless steel, *Corrosion* 54 (1998) 628–634.
- [16] M. Fregonese, H. Idrissi, H. Mazille, L. Renaud, Y. Cetre, Initiation and propagation steps in pitting corrosion of austenitic stainless steels: monitoring by acoustic emission, *Corros. Sci.* 43 (2001) 627–641.
- [17] J.B. Pethica, R. Hutchings, W.C. Oliver, Hardness measurement at penetration depths as small as 20 nm, *Philos. Mag. A* 48 (1983) 593–606.
- [18] E. Lilleodden, W. Bonin, J. Nelson, W.W. Gerberich, In-situ imaging of unload indents into GaAs, *J. Mater. Res.* 10 (1995) 2162–2165.
- [19] D.F. Bahr, D.E. Kramer, W.W. Gerberich, Non-linear deformation mechanisms during nanoindentation, *Acta Mater.* 46 (1998) 3605–3617.
- [20] S.K. Venkataraman, D.L. Kohlstedt, W.W. Gerberich, Continuous microindentation of passivating surfaces, *J. Mater. Res.* 8 (1993) 685–688.
- [21] X. Gao, Displacement burst and hydrogen effect during loading and holding in nanoindentation of an iron single crystal, *Scr. Mater.* 53 (2005) 1315–1320.
- [22] M.J. Cordill, N.R. Moody, W.W. Gerberich, The role of dislocation walls for nanoindentation to shallow depths, *Int. J. Plast.* 25 (2009) 281–301.
- [23] K.A. Nibur, D.F. Bahr, B.P. Somerday, Hydrogen effects on dislocation activity in austenitic stainless steel, *Acta Mater.* 54 (2006) 2677–2684.
- [24] A. Barnoush, H. Vehoff, Recent developments in the study of hydrogen embrittlement: hydrogen effect on dislocation nucleation, *Acta Mater.* 58 (2010) 5274–5285.
- [25] W.C. Oliver, G.M. Pharr, An improved technique for determining hardness and elastic modulus using load and displacement sensing indentation experiments, *J. Mater. Res.* 7 (1992) 1564–1583.
- [26] M.F. Doerner, D.S. Gardner, W.D. Nix, Plastic properties of thin films on substrates as measured by submicron indentation hardness and substrate curvature techniques, *J. Mater. Res.* 1 (1986) 845–851.
- [27] M. Pang, D.F. Eakins, M. Norton, D.F. Bahr, Structural and mechanical characteristics of anodic oxide films on titanium, *Corrosion* 17 (2001) 523–531.
- [28] D.F. Bahr, T.C. Nelson, N.I. Tymiak, W.W. Gerberich, The mechanical behavior of a passivating surface under potentiostatic control, *J. Mater. Res.* 12 (1997) 3345–3353.
- [29] W.W. Gerberich, S.K. Venkataraman, H. Huang, S.E. Harvey, D.E. Kohlstedt, The injection of plasticity by millinewton contacts, *Acta Metall. Mater.* 43 (1995) 1569–1576.
- [30] Q. Yang, J.L. Luo, The effects of hydrogen on the breakdown of passive films formed on Type 304 stainless steel, *Thin Solid Films* 371 (2000) 132–139.
- [31] J.P. Hirth, Effects of hydrogen on the properties of iron and steel, *Metall. Trans. A* 11 (1980) 861–890.
- [32] J.G. Yu, J.L. Luo, P.R. Norton, Effects of hydrogen on the electronic properties and stability of the passive films on iron, *Appl. Surf. Sci.* 177 (2001) 129–138.
- [33] J.G. Yu, J.L. Luo, P.R. Norton, Electrochemical investigation of the effects of hydrogen on the stability of the passive film on iron, *Electrochim. Acta* 47 (2002) 1527–1536.
- [34] T. Shibata, Passivity breakdown and stress corrosion cracking of stainless steel, *Corros. Sci.* 49 (2007) 20–30.